Hierarchical Growth of ZnO Particles by a Hydrothermal Route

F Bamiduro, M B Ward, R. Brydson, S J Milne.

Institute of Materials Research (IMR), School of Process, Environmental and Materials Engineering, University of Leeds, Leeds LS2 9JT, UK

ABSTRACT: The crystallization of ZnO microrods by hydrothermal treatment of a suspension formed from reaction of zinc acetate and sodium hydroxide has been examined using scanning and transmission electron microscopy as a function of hydrothermal reaction time. Polycrystalline hexagonal ZnO microrods first appeared after 0.5 h reaction time at 120 °C. These early stage rods were composed of stacks of hexagonal layers, each ~ 50 nm in thickness containing closely aligned assemblies of nanocrystallites < 20 nm in size.   A further growth stage involving smaller pseudo-hexagonal columns nucleating and growing along <0001> from the (0001) basal layers of preformed polycrystalline hexagonal microrods was identified. For reaction times > 3h, the microrods were single crystals, as identified by TEM lattice imaging and electron diffraction, and many were in the form of double rods.

Introduction

Zinc oxide has attracted considerable attention in recent years due to the distinctive properties of nanostructured forms of this wide band gap semiconductor which may be exploited in new electronic and photonic applications.[1-5] Conventional uses of ZnO include varistors, piezoelectrics, sensors,

photocatalysts, cosmetics and sunscreens.[6, 7, 8] Zinc oxide typically crystallises with the wurtzite hexagonal structure.[9] Physical and electronic properties of ZnO are dependent on particle size and morphology. Hydrothermal synthesis is one of the most popular solution synthesis routes and offers the opportunity to produce ZnO particles in a variety of shapes, and sizes from the micro- to nanoscale.[2,10-12] For example, platelets, flower–like clusters, tetrapods and multiple branched structures are reported.[13-17] Control of particle shape and size may be achieved by variation of: zinc precursor reagent type and concentration, pH, reaction temperature and pressure.[5,10-14,21] Growth control additives, alternatively referred to as capping agents or structure-directing agents, are often employed to moderate ZnO particle shape. Additives include: cetyltrimethylammonium bromide (CTAB), sodium dodecyl sulphate, ethylenediamine, hexamethylenetetramine and citric acid.[18-23]

The effects of the type of precursor zinc reagent have been reported by several groups. For example secondary particles 160 nm in diameter composed of 5 nm primary crystallites was formed from zinc nitrate, but by using zinc acetate, a mixture of 15 nm equiaxed and elongated 40 nm by 15 nm particles was obtained.[24] It was suggested that the differences were related to the chelating effects of the acetate group in hindering the interaction of a polyvinyl butyrate additive with zinc ions during the growth phase.[24] It has been reported that changes to the ratio of OH^- to Zn^{2+} have only a minor effect on the size of ZnO nanorods.[5] Others have varied the ratio of NaOH to zinc acetate; flower-like structures were obtained at a OH/Zn ratio of 8.2, these increased in size as the OH/Zn ratio increased to 10 (starting pH was not reported). At OH/Zn ratios of 11-12, single hexagonal rods 1-2 um in length were produced. The authors suggested growth occurred from solutions supersaturated with respect to $Zn(OH)_4^{2-}$.[25] The occurrence of a hexagonal prismatic morphology [26-31] is generally assumed to be a consequence of surface energy effects favouring the development of {10-10} and {0001} crystal faces.

This paper commences with a description of particle size and morphology in a sample produced from a 'standard' 12 reaction at 120 °C followed by an examination of particle evolution at shorter reaction times. In contrast to a number of previous papers on hydrothermal synthesis of ZnO, no growth control additives were employed..

Experimental

Zinc acetate dihydrate, 0.0342 mol, (Sigma-Aldrich, $\geq$ 99.0 % purity) was dissolved in 100 ml distilled water. A precipitate was formed by by adding 100 ml of aqueous NaOH (0. 18 M) to the zinc acetate solution. Addition of NaOH solution (2M) was required to bring the suspension to pH = 9 (total sample volume = 217 ml). The amount of NaOH required to attain pH = 9 was 0.052 mol. Given that the anticipated hydrolysis reactions to form $Zn(OH)_2$ or $ZnO + H_2O$ (Equations 1-2 below) involve a 1:2 molar ratio of $Zn(OOCCH_3)_2$ to base, the starting NaOH content (0.052 mol) is slightly below the stoichiometric amount (0.068 mol) to react with 0.0342 mol of zinc acetate.

The pressure vessel containing the suspension was heated at a rate of 5 ^{0}C/min to a temperature of 120 °C in a box furnace, and maintained at this temperature for 12 h, after which it was cooled at 5 ^{0}C/min to room temperature. These experiments were repeated using shorter reaction times, 0.5, 1, 2, 3, 6 h. The precipitate from the overall hydrolysis (and dehydration) reactions within the pressure vessel was separated from the solution by centrifugation at 6000 rpm for 5 min. The sediment was re-suspended in distilled water using ultrasonic agitation; the washing-centrifugation sequence was repeated a further five times, with a final wash carried out in methanol.

X-ray diffraction (XRD) of the dried powders was performed using a Philips PANanalytical X'Pert diffractometer. Particle size and shape was observed using scanning electron microscopy (SEM, LEO 15300); structural details were revealed by transmission electron microscopy, TEM (FEI Tecnai F20 FEG-TEM) operated at 200 kV and equipped with a Gatan Orius SC600A CCD camera.

3

Results and Discussion

X-ray powder diffraction confirmed the product of the standard reaction at 120°C for 12 h to be single-phase ZnO crystallizing with the hexagonal wurtzite structure, Figure 1. Typical SEM images of the particles are shown in Figure 2.
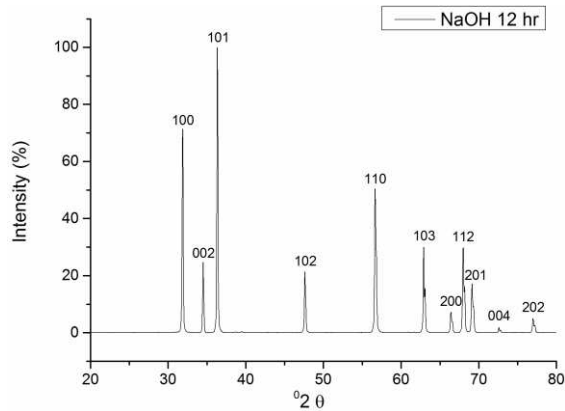

Figure 1: X-ray powder diffraction patterns of the products of hydrothermal reaction at 120 °C for 12 h confirming single-phase wurtzite ZnO powders (international centre for diffraction data (ICDD) File No. 04-008-8198
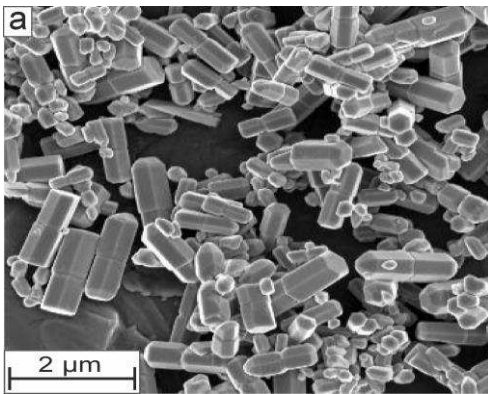

Figure 2: SEM micrographs of ZnO produced by hydrothermal reaction at 120 °C for 12 hr

4

The ZnO powder was composed of a mixture of particle sizes and shapes, categorised as: Type I particles ≤ 0.3 μm in size; Type II hexagonal rod-like particles, length ≤ 0.6 μm; Type III double hexagonal rods, total length ≤ 1.8 μm, Figure 2. The relative amounts of each particle type were estimated by analysing multiple SEM images: Type 1 particles constituted ≤ 10 % of the sample, Type II ≤ 20 %, Type III ≤ 70% (with no significant difference for reaction times 1-12 h).

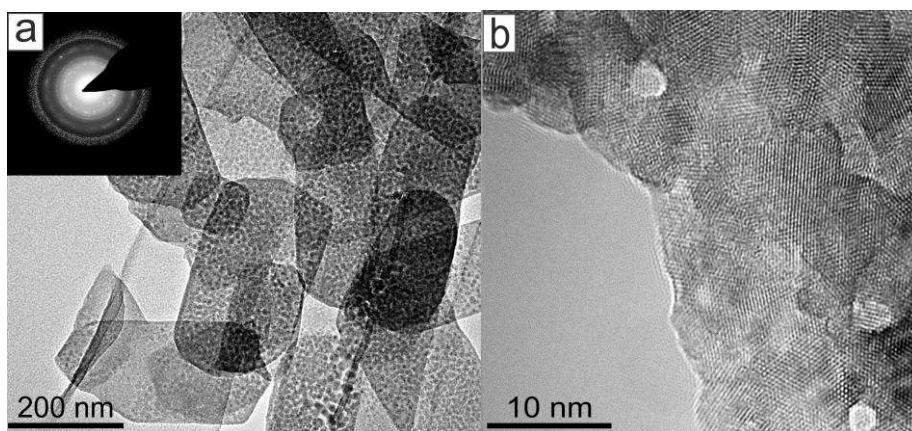**Figure 3: TEM micrographs of Type I particles (120 °C for 12 h) showing: (a) < 300 nm particles and (b) a < 10 nm polycrystalline substructure identified from non-oriented lattice imaging of (0002) planes. Nanopores appear as regions of light contrast.**

Transmission electron microscopy of Type I particles, some of which were lozenge shaped, contained a substructure of < 20 nm primary crystallites, Figure 3a. Pores < 5 nm in size were identified in a number of particles, Figure 3b. Levels of mesoporosity (5-50 nm) in the bulk powders were investigated using gas adsorption porosimetry, Figure 4, indicating 5.7 vol% mesoporosity. Type II single and Type III double microrods were shown by selected area electron diffraction to be single crystals, Figures 5 and 6 (double rods were composed of two coherent single crystal rods). Lattice imaging revealed planes, with measured d-spacing equivalent to the (0002) planes of ZnO, running perpendicular to the length of the rods, confirming preferential growth along <0001>. The sides of

5

well-faceted hexagonal rods thus correspond to the {10 -10} family of planes, and the basal section to the {0001} planes, as has been reported for ZnO prepared from other synthesis conditions.[26-31]
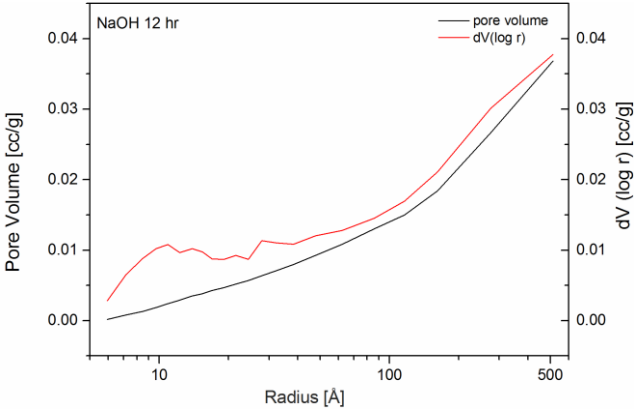
Figure 4: Results of gas porosimetry confirming the presence of mesopores (see also Figure 2 in ZnO particles (120 °C for 12 h)
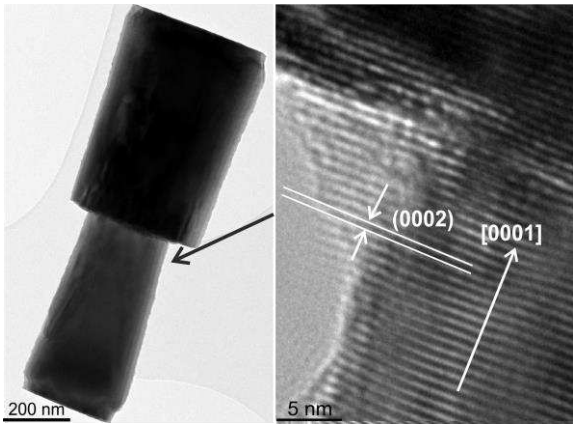
Figure 5: TEM micrograph of double ZnO rod and contiguous (0002) ZnO lattice planes running across a twin rod interface in Type IIIa particles (120 °C for 12 h)

6
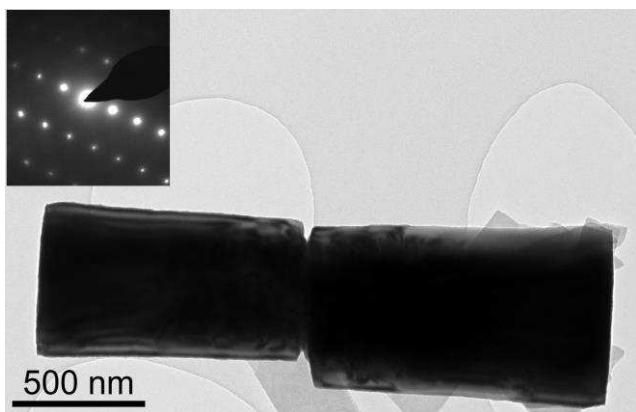
Figure 6 TEM micrograph of a Type IIIb ZnO double rod. Inset shows selected area electron diffraction pattern, confirming rods to be single crystals.

Figure 7 XRD patterns as a function of hydrothermal reaction time: (a) 0 h; (b) 1 h and (c) 3 h. Peaks assigned to zinc acetate in the 0 h sample are marked X, ICDD file no. 00-033-1467

The Type III rods may be divided into two sub-groups, IIIa and IIIb. The Type IIIa double rods, Figure 5, have a sharp interface at the junction between component rods, and lattice planes run coherently across the interface.[28,30,33] Other workers have proposed that this type of rod is a result of crystallographic twinning in which growth initiates at a silicon-rich impurit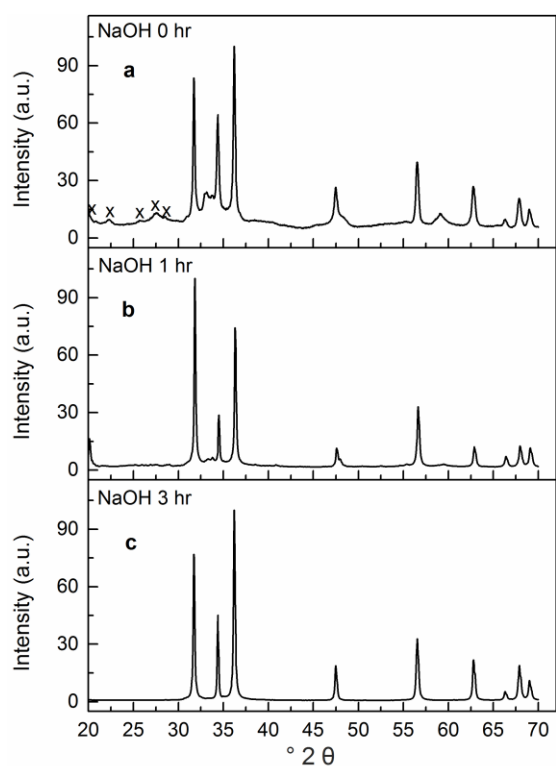y phase detected by TEM at the interface between two rods.[33] However silicon is commonly detected by TEM-EDX irrespective of the specimen composition, and is generally considered to originate from instrumental factors. We found no difference in the background silicon signal (compared to the intensity of copper EDX peaks from the specimen grid) at different points across double rods.

Type IIIb double rods, Figure 6, have a less regular interfacial junction than Type IIIa, and most probably result from the coming together of two individual Type II rods, aligned along <0001>. Opposing polarities of basal terminations and selective adsorption of $[Zn(OH)_4]^{2-}$ species   are reported to be responsible for this type of alignment.[4, 30,31] However it was not possible to measure polarities to confirm this hypothesis.

Insights into the ZnO particle growth mechanisms were gained by examining particles produced at a series of shorter hydrothermal reaction times < 12 h, and by examining the '0 h' precipitate that provided the feedstock for hydrothermal reaction.

X-ray diffraction revealed that the 0 h precipitate contained crystalline ZnO, along with minor amounts of secondary-crystalline phases which could not be identified unambiguously, although some reflections were consistent with zinc acetate, Figure 7a, indicating incomplete reaction. Hydrothermal reaction at 120 °C for > 1 h eliminated the secondary phases from the XRD pattern, giving a single-phase ZnO product, Figure 7b,c.

SEM micrographs for as-precipitated 0 h sample, and the products from hydrothermal reaction after 0.5 h, 1 h, and 6 h are presented in Figure 8. The   0 h sample was composed of large irregular

flake-like particles, > 10 μm in size, with a sub-micron surface topography, Figure 8a; ; there was no evidence of hexagonal rod formation. Hexagonal rods similar to Type II and III, described above for the 12 h reactions, first appeared in the 0.5 h reaction product, but these constituted only ≤ 10 % of the sample (projected area in SEM micrographs); most of the sample was still in the form of flake-like particles, Figure 8b. After reaction for 1 h, the sample was predominantly (~ 90 %) rod-like, but many of the rods had not yet developed a well-defined hexagonal morphology, Figure 9c. Well-defined hexagonal rods were produced after ≥ 3 h, Figure 8d.
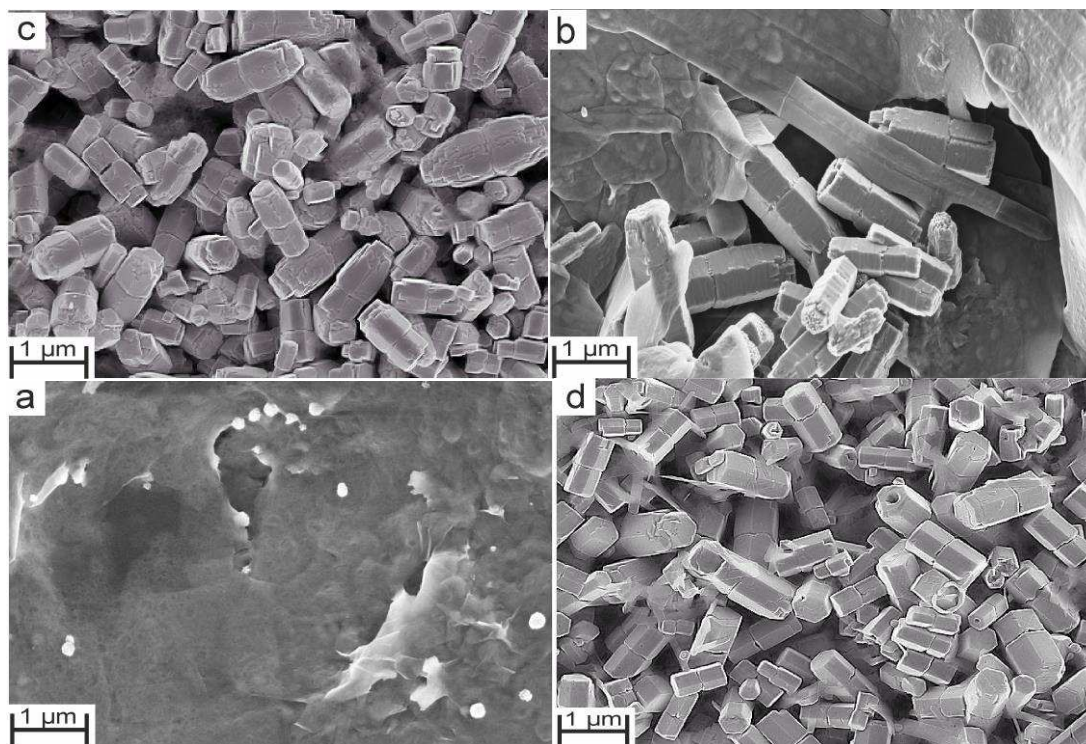

Figure 8: SEM micrographs of ZnO produced at reaction times: (a) 0 h (as-precipitated product prior to hydrothermal processing); (b) 0.5 h; (c) 1 h; and (d) 3 h

The rods present in the 0.5 h product are interpreted as representing the early stages of Type II/III particle formation. Higher magnification SEM, Figure 9a,b, revealed the 0.5 h rods were constructed from stacks of hexagonal layers, each layer estimated at ≤ 50 nm in thickness with lateral dimensions ≤ 600 nm. The side faces of the individual hexagonal layers were relatively smooth but the basal surfaces had a clearly defined nanoscale sub-structure.

From SEM examination ~ 50 % of the rods in the 0.5 h sample showed longitudinal growth of microrods proceeding in a discontinuous manner from an existing hexagonal rod as in Figure 9a,b. It is presumed that later re-crystallisation converts the segmented, polkycrystalline hexagonal stacks of aligned nanocrystallites into single crystals (with sharp SAED reflections, Figure 6).
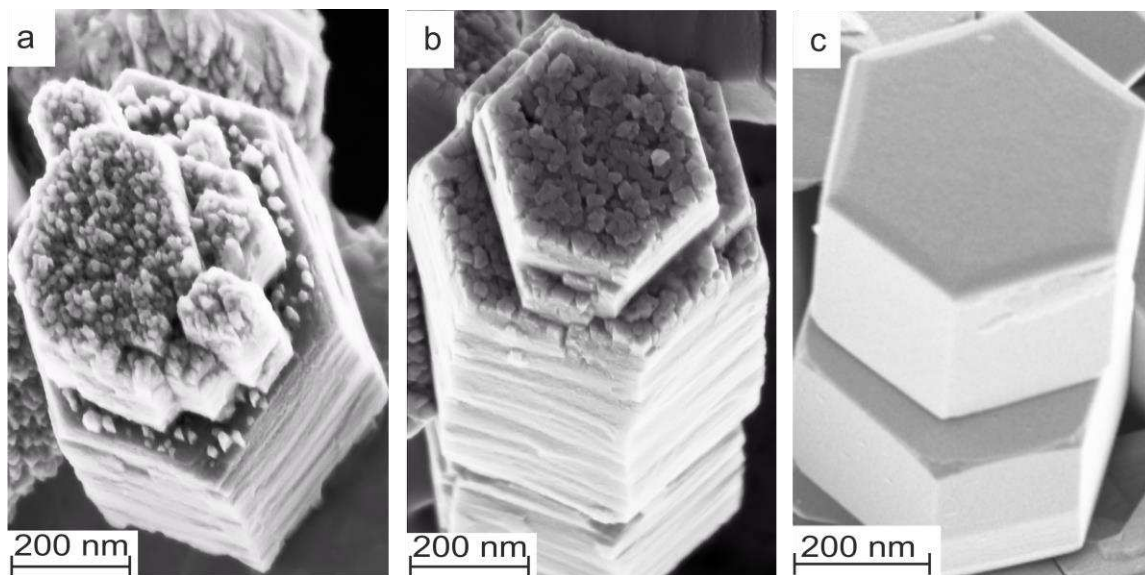

Figure 9: SEM micrographs showing incremental stages in the development of a Type IIIa ZnO double rod; (a) and (b) are structures formed in the same 0.5 h hydrothermal reaction product; (c) represents recrystallised double rod in a 3 h reaction.
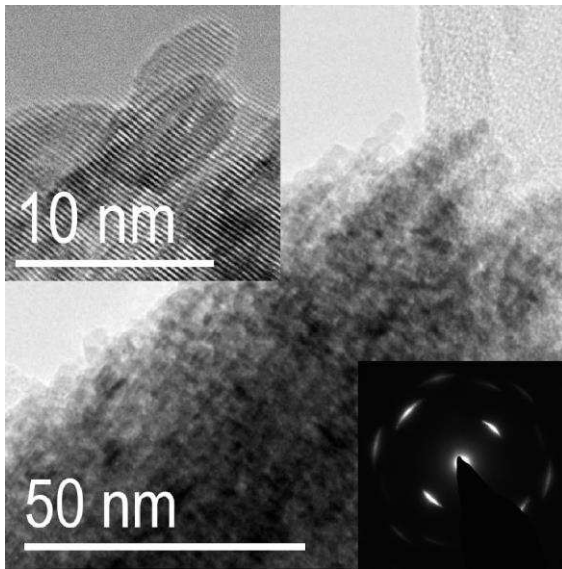
Figure 10 TEM image of rod similar to shown in Figure 9a, 0.5 h reaction time showing nanorods of ZnO collectively aligned in longitudinal growth direction of bulk microrod. Insets show lattice fringing (top) and selected area electron diffraction down [0001] zone axis with streaking to reflections indicating a mutual misalignment of ≤ 20° in nanorod alignment. Arrow indicates longitudinal growth direction.

The progression in the formation of Type IIIa rods is illustrated by the three micrographs shown in Figures 9a-c (Fig 9c is from a 3 h sample). A schematic of the overall ZnO growth processes for the reaction of $Zn(CH_3COO)_2$ and NaOH is presented in Figure 10. The principal stages are: A) nucleation and growth of ZnO primary nanorods < 20 nm in size, aligned in a pseudo <0001> direction and assembled in hexagonal layers < 1 μm in width and ~ 50 nm in depth; B) stacking of these hexagonal layers into segmented microrods; C) heterogeneous nucleation and growth of sub-columns from the pre-formed hexagonal stacks, in the <0001> direction; D) re-crystallisation to form single crystal hexagonal microrods Although the results have identified aspects of the growth process, specifically in relation to the intermediate stage substructure that leads to well-crystallised hexagonal rods, there remains uncertainty as to the reasons why double rods form. As mentioned above arguments regarding opposed polarity terminations have been proposed, which could account for Type IIIb double

11

rods. Alternatively, a mechanism akin to crystallographic twinning has been suggested, which more closely agrees with the incremental growth steps identified in Figure 9 - that may relate to Type IIIa double rods. Indeed, a combination of growth mechanisms may operate, in which early stage rods with opposed polarity basal terminations co-join, followed by subsequent step-wise growth along opposed <0001> directions in the manner shown in Figure 9.

Some of the isolated Type I < 300 nm particles first identified in the 12h sample were lozenge shaped and may be forerunners of the hexagonal lamellae that stack to form hexagonal rods (Figure 9). The proportion of Type I was generally ≤ 10 % with no obvious trend with changing reaction times 1-12 h. At higher reaction temperatures, > 120 °C, and/or longer reaction times > 12 h, the hexagonal Type II and III microrods became larger and Type I particles were absent, inferring they were consumed by an Ostwald ripening process in later stages of particle development.
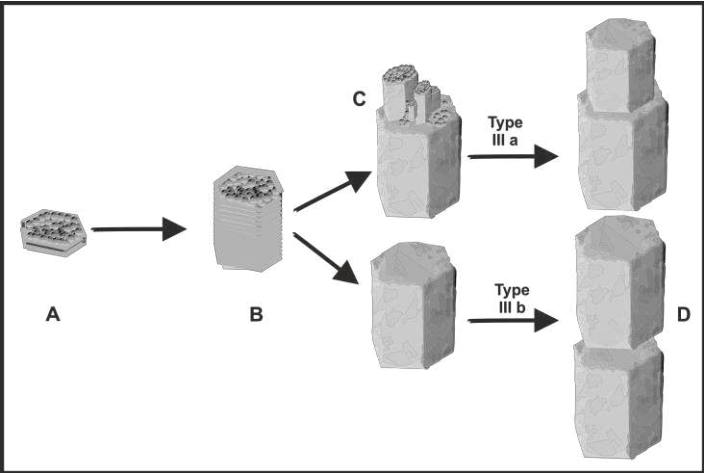

Figure 11: Schematic growth process of ZnO particles based on evidence gathered from SEM and TEM

The existence of ZnO   in the '0h' precipitate, infers rapid conversion of a $Zn(OH)_2$ hydrolysis product to ZnO (Equations 1 and 2).

$$Zn(Ac)_2 + 2OH^- + 2Na^+ = Zn(OH)_2 + 2NaAc \qquad (Ac = CH_3COO) \qquad \text{Equation 1}$$

$$Zn(OH)_2 = ZnO(s) + H_2O \qquad\qquad\qquad\qquad\qquad \text{Equation 2}$$

Hydroxyl complex ions $Zn(OH)_4^{2-}$ may also be present during the reaction due to further hydrolysis of $Zn(OH)_2$. Direct crystallization of ZnO from aqueous solution has been reported previously. [40]

There are, to our knowledge, no prior reports showing evidence of early stage nucleation and growth processes in hydrothermal reactions involving zinc acetate and sodium hydroxide. The specific sequence of growth stages revealed by electron microscopy shows a distinctive hierarchical growth sequence, involving transient stage microrods composed of polycrystalline, closely aligned sub crystals. There are several reports of different types of hierarchical growth from other reaction conditions.[18,32,34-36]   For example, a two stage ZnO growth process is   reported in the synthesis of ZnO nanowires, involving clustering of primary nanoparticles into bunches, promoted by long chain surfactants, amines or citrates.[31,33]   In the present case, no growth control additives were used. Hexagonal ZnO plates resulted from a two stage assembly of nanoparticles where the amine, CTAB acted as a template.[34] Clusters of ZnO nanowires were formed in the presence polyvinyl pyrrolidone (PVP).[35] Branched, impeller-like structures were formed on glass substrates, involving clusters of inclined nanorods growing off micron scale ZnO pillars.[36]   Bipods similar to the present Type III particles   from NaOH were formed from zinc nitrate, ethyleneglycol and urea; lattice imaging showed the rods to be aligned

13

along <0001>, and an inversion domain boundary was proposed in which particles grew in opposed [0001] and [000-1] directions from a silicon rich region thought to arise from silicon impurities, as discussed earlier in the text.[33]

Conclusions

Suspensions produced by titration of zinc acetate and sodium hydroxide were processed in an autoclave at a temperature of 120 °C for different dwell times, ≤ 12 h. The product of hydrothermal reaction for 12 h contained a variety of particle types: double hexagonal rods of total length ≤ 1.8 μm and width ≤ 0.6 μm formed the main fraction (≥ 70 %) but single hexagonal microrods < 0.5 μm in length, and nanostructured particles ≤ 0.3 μm in size were also present.

Insights into growth mechanisms were gained from SEM and TEM examination of particles formed at incremental reaction times < 12 h. This revealed a hierarchical growth process, commencing with the formation and assembly of nano ZnO crystallites. Hexagonal ZnO microrods first formed after 0.5 h, growing along the <0001> direction by stacking of hexagonal layers each ~ 50 nm in depth composed of oriented nanorod particles, ≤ 20 nm in width. Evidence of hierarchical growth from the basal layers of well-developed hexagonal rods, involving columns of closely aligned crystallites, was demonstrated as a possible growth mechanism leading to double rod formation.

14

REFERENCES

(1) A. P. Alivisatos, Naturally Aligned Nanocrystals, Science, **298**, 736- 737 (2000).

(2)B. Liu, H. C. Zeng, Hydrothermal Synthesis of ZnO Nanorods in the Diameter Regime of 50 nm, J. Am. Chem. Soc., **125**, 4430 – 4431 (2003).

(3) D. Kisailus, B. Schwenzer, J. Gomm, J.C. Weaver, D.E.Morse, Kinetically Controlled Catalytic Formation of Zinc Oxide Thin Films at Low Temperature, J. Am. Chem. Soc., **128**, 10276-10280 (2006).

(4) M. Bitenc, P. Podbrscek, Z.C. Orel, M.A. Cleveland, J.A. Paramo, R.M. Peters, Y.M. Strzhemechny, Correlation between Morphology and Defect Luminescence in Precipitated ZnO nanorod Powders, Crystal Growth & Design **9**(2), 997 – 1001 (2009).

(5) K. Elen, H. Van den Rul, A. Hardy, K.M. Van Bael, J. D'Haen, R. Peeters, D. Franco, J. Mullens, Hydrothermal synthesis of ZnO nanorods: a statistical determination of the significant parameters in view of reducing the diameter, Nanotech. **20**, 1 – 8 (2009).

(6) W. Onreabroy, N. Sirikulrat, A.P. Brown, C.H. Hammond, S.J. Milne, Properties and Intergranular Phase Analysis of a ZnO–CoO–Bi_2O_3 Varistor, Solid State Ionics **177**, 411-20 (2006).

(7) R. Kitture, S.J. Koppikar, R. Kaul-Ghanekar, S.N. Kale, Catalyst efficiency, photostability and reusability study of ZnO nanoparticles in visible light for dye degradation, J. Phys. & Chem. Solids **72**, 60–66 (2011).

(8) H. Zhang, B. Chen, H. Jiang, C. Wang, H. Wang, X. Wang, A strategy for ZnO nanorod mediated multi-mode cancer treatment, Biomaterials, **32**, 1906 – 1914 (2011).

(9) J. Wróbel, J. Piechota, Structural properties of ZnO polymorphs, Physica Status Solidi (b) **244**, 1538 – 1543 (2007).

(10) L. W. Suchanek, E.R. Riman, Hydrothermal synthesis of advanced ceramic powders, Adv. in Sc & Tech. **45**, 184-193 (2006).

(11) S. Baruah, D. Joydeep, Hydrothermal growth of ZnO nanostructures, Sci. Technol. Adv. Mater., **10**, 1-18 (2009).

(12) X. Ma, H. Zhang, Y. Ji, J. Xu, D. Yang, Sequential occurrence of ZnO nanopaticles, nanorods, and nanotips during hydrothermal process in a dilute aqueous solution, Mat. Lett. **59,** 3393 – 3397 (2005).

(13) X. Gao, X. Li, W.J. Yu, Flowerlike ZnO Nanostructures via Hexamethylethylenetetramine-Assisted Thermolysis of Zinc-Ethylenediamine, J. Phys. Chem. B, **109,** 115 – 1161 (2005)

(14) A. Wei, X.W. Sun.; C.X. Xu, Z.L. Dong, Y. Yang, S.T. Tan, W. Huang, Growth mechanism of tubular ZnO formed in aqueous solution, Nanotechnology, **17,** 1740 – 1744 (2006).

(15) Q. Ahsanulhaq, J.M. Kim, N.K. Reddy, Y.B. Hahn, Growth mechanism and characterization of rose-like microspheres and hexagonal microdisks of ZnO grown by surfactant-free solution method, J. Ind. Eng. Chem. **14**, 578 – 583 (2008).

(16) Q.-P. Luo, B.-X. Lei, X.-Y. Yu, D.B. Kuang, C-Y. Su, Hiearachical ZnO rod-in-tube nano-architecture arrays produced via a two-step hydrothermal and ultrasonication process, J. Mat. Chem., **21**, 8709 – 8714 (2011).

17

(17) H. Wang, J. Xie, K. Yan, M. Duan, M., Growth Mechanism of Different Morphologies of ZnO Crystals Prepared by Hydrothermal Method, J. Mater. Sci. Technol., **27**, 153-158 (2011).

(18) L. Hui, Y. Zhang, H. Liu, J.; Wang, Large ZnO Mesocrystals of Hexagonal Columnar Mrphology Derived from Liquid Crystal Templates, J. Am. Ceram. Soc., **94**, 3267 – 3275 (2001)

(19) M. Yin, Y. Gu, I.L. Kuskovsky, T. Andelman, Y. Zhu, G.F. Neumark, S. O'Brien, Zinc Oxide Quantum Rods, S. J. Am. Ceram. Soc., **126**, 6206-6207 (2004).

(20) H. Zhang, D. Yang, Y. Ji, X, Ma, J. Xu, D. Que, Low Temperature Synthesis of Flowerlike ZnO Nanostructures by Cetyltrimethylammonium Bromide-Assisted Hydrothermal Process, Physical Chem. B., **108**, 3955 (2004).

(21) S.A. Morin, F.F. Amos, S. Jin, Biomimetic Assembly of Zinc Oxide Nanorods onto Flexible Polymers, J. Am. Ceram. Soc., **129**, 13776 (2007).

(22)D. Polsongkram, P. Chamninok, S. Pukird, L.O. Chow, G.C. Lupan, H. Khallaf, S. Park, A. Schulte, Effect of synthesis conditions on the growth of ZnO nanorods via hydrothermal method, Physica B **403,** 3713 (2008).

(23) B. Coasne, A. Mezy, R.J.M. Pellenq, D. Ravot, J.C. Tedenac, Zinc Oxide Nanostructures Confined in Porous Silicas, J. Am. Ceram. Soc., **31,** 2185 (2009).

(24) M. Distaso, R.N.K. Taylor, N. Taccardi, P. Wasserscheid, W. Peukert, Influence of the Counterion of the Synthesis of ZnO Mesocrystals under Solvothermal Conditions, Chem. Eur. J., **17**, 2923 (2011).

(25) Z. Zhang, J. Mu, Controllable synthesis of flower- and rod-like ZnO nanostructures by simply tuning the ratio of sodium hydroxide to zinc acetate Nanotechnology **18**, 075606 (2007)

(26) F. N. Hamedani, A.R. Mahjouba, A.A. Khodadadi, Y. Mortazavi, Microwave assisted fast synthesis of various ZnO morphologies for selective detection of CO, CH4 and ethanol, Sensors & Actuators B **156**, 737 (2011).

18

(27) C.-Y. Kao, C.-L. Hsin, C.-W. Huang, S.-Y. Yu, C.W. Wang, P.-H. Yeh, W.-W Wu, High-yield synthesis of ZnO nanowire arrays and their opto-electrical properties, Nanoscale **4**, 1476-1480 (2012).

(28) B.G. Wang, E.W. Shi, W.Z. Zhong, Twinning Morphologies and Mechanisms of ZnO Crystallites under Hydrothermal Conditions, Cryst. Res. Technol., **33**, 937 (1998).

(29) Q. Li, V. Kumar, Y. Li, H. Zhang, T.J. Marks, R.P.H. Chang, Fabrication of ZnO Nanorods and Nanotubes in Aqueous Solutions, Chem. Mater., 17, 1001 (2005).

(30) H. Jiang, J. Hu, F. Gu, C.J.; Li, Self-assembly of solid or tubular ZnO rods into twinning microprisms via a hydrothermal route, J. Alloys and Compounds **478,** 550 (2009).

(31) Y. Liu, H. Lv, S. Li, G. Xi, X. Xing, Adv. Powder Technol., **22**, 784 (2011)

(32) S. Sharma, M.K. Sunkara, Direct Synthesis of Gallium Oxide Tubes, Nanowires, and Nanopaintbrushes, J. Am. Chem. Soc., **124**, 12288 (2002)

(33) M. Bitenc, G. Drazic, Z.C. Orel, Characterization of Crystalline Zinc Oxide in the Form of Hexagonal Bipods, Crystal Growth & Design **10**, 830 (2010)

(34) H. Tang, J.C. Chang, Y. Shan, S-T Lee, Surfactant-Assisted Alignment of ZnO Nanocrystals to Superstructures, J. Phys. Chem., B **112**, 4016 (2008)

(35) Y. Feng, Y. Peng, G.-Y. Chen, B. Deng, A.-W. Xu, Facile Solution Synthesis and Characterization of ZnO Mesocrystals and Ultralong Nanowires from Layered Basic Zinc Salt Precursor, J. Phys. Chem. C **113,** 10407 (2009)

(36) T. Zhang, W. Dong, M. Keeter-Brewer, S. Konar, R.N. Njabon, Z.R. Tian, Site-Specific Nucleation and Growth Kinetics in Hierachical nanosyntheses of Branched ZnO Crystallites J. Am. Chem. Soc., **128**, 10960 (2006)

(37) Y. Zhang, M. Muhammed, Critical evaluation of thermodynamics of complex formation of metal ions in aqueous solutions - VI. Hydrolysis and hydroxo-complexes of Zn^{2+} at 298.15 K, Hydrometallurgy **60**, 215 (2001).

19

(38) A, Degen, M. Kosec, Effect of pH and impurities on the surface charge of zinc oxide in aqueous solution, J. Eur. Ceram. Soc., **20**, 667 (2000)

(39) Shaw, Duncan J. Introduction to Colloid and Surface Chemistry, Butterworths: London, 1985, 148 - 195

(40) H. Zhang, B. Chen, H. Jiang, C. Wang, H. Wang, X. Wang, Biomaterials **32**, 1906 - 1914 (2011)

(41) R.H. Petrucci, S.W. Harwood, G. F. Herring, D.J. Madura, General Chemistry: Principles and Modern Applications: Pearson Education: New Jersey, 2007; Chapter 18, pp 761-770

(42) I.O. Oladeji, L. Chow, A study of the effects of ammonium salts on chemical bath depositedzinc sulphide thin films, Thin Solid Films **339**, 148-153 (1999)

(43) Y. Zhang, M. Muhammed, Hydrometallurgy **60**, 215–236 (2001)

X